

Modeling Symmetric Positive Definite Matrices with An Application to Functional Brain Connectivity

Zhenhua Lin,^{*} Dehan Kong[†] and Qiang Sun[‡]

Abstract

In neuroscience, functional brain connectivity describes the connectivity between brain regions that share functional properties. Neuroscientists often characterize it by a time series of covariance matrices between functional measurements of distributed neuron areas. An effective statistical model for functional connectivity and its changes over time is critical for better understanding the mechanisms of brain and various neurological diseases. To this end, we propose a matrix-log mean model with an additive heterogeneous noise for modeling random symmetric positive definite matrices that lie in a Riemannian manifold. The heterogeneity of error terms is introduced specifically to capture the curved nature of the manifold. We then propose to use the local scan statistics to detect change patterns in the functional connectivity. Theoretically, we show that our procedure can recover all change points consistently. Simulation studies and an application to the Human Connectome Project lend further support to the proposed methodology.

Keywords: change point, functional connectivity, Riemannian manifold, sure coverage property.

1 Introduction

Understanding the functional brain connectivity is critical for understanding the fundamental mechanisms of brain, how it works, and various neurological diseases. It has attracted great interest recently. For instance, the Human Connectome Project investigates the structural and functional connectivity in order to diagnose cognitive abilities of individual subjects. Functional connectivity can be defined as temporary statistical dependence between spatially remote neurophysiological events (Friston, 2011), and has been observed to be dynamic in nature, even in the resting state (Hutchison et al., 2013). In practice, neuroscientist often characterize the dynamic functional connectivity by a series of symmetric positive definite (SPD) covariance matrices between functional measurements of neuronal

^{*}Department of Statistics, University of California, Davis.

[†]Department of Statistical Sciences, University of Toronto.

[‡]Address for correspondence: Department of Statistical Sciences, University of Toronto, Toronto, Ontario M5S 3G3, Canada; E-mail: qsun@utstat.toronto.edu.

activities across different regions in human brain. Establishing appropriate dynamic models is critical for understanding fundamental mechanisms of brain networks and has attracted much attention in neuroscience recently (Xu and Lindquist, 2015; Hutchison et al., 2013).

However, little has been done in the statistics community for investigating dynamic changes of functional connectivity over time. The non-Euclidean structure of covariances has introduced significant challenges to the development of proper statistical models and their analysis. Indeed, all SPD matrices form a nonlinear Riemannian manifold, which is referred to as the SPD manifold. Motivated by the SPD manifold structure under the Log-Euclidean metric (Arsigny et al., 2007), we use the matrix logarithm to embed the SPD matrices into a Hilbert space – an Euclidean space up to a symmetric structure, to be concrete. We then model the transformed random SPD matrix using a mean model with an additive heterogeneous noise. The heterogeneous error depends on the tangent space of the mean SPD matrix and thus takes the curved structure of the SPD manifold into account. Our work refines the previous work by Chiu et al. (1996), whose model does not respect the original manifold structure.

Built on this statistical model, we then propose to use a form of local scan statistics to detect multiple change patterns that are present in the functional brain connectivity over time. To the best of our knowledge, ours is the first work on the study of change point detection for SPD manifold-valued data. Although the proposed method is primarily motivated by discovering change patterns in fMRI, it has the potential to be applied to many other applications, such as diffusion tensor imaging (Dryden et al., 2009) and longitudinal data analysis (Daniels and Pourahmadi, 2002).

1.1 Related Literature

Change point detection with at most a single change point has been widely studied in the literature. When the distributions of the data are assumed to be known, score- or likelihood-based procedures can be applied (James et al., 1987). Bayesian and nonparametric approaches have also been proposed, see Carlstein et al. (1994) for a review. More recently, Chen and Zhang (2015) proposed a graph based approach for nonparametric change point detection. When there are multiple change points, the problem becomes much more complicated. Some popular approaches include the exhaustive search with Schwarz criterion (Yao, 1988), the circularly binary segmentation (Olshen et al., 2004) and the fused lasso method (Tibshirani and Wang, 2007). In genomics, these techniques have been exploited to study DNA copy number variations, see Olshen et al. (2004); Zhang and Siegmund (2007); Tibshirani and Wang (2007) among others. However, none of the above methods deals with Riemannian data.

There have been a few works on Riemannian data analysis in the statistics literature. For example, Schwartzman (2006) proposed several test statistics for comparing the means of two populations of symmetric positive definite matrices. Zhu et al. (2009) developed a semiparametric regression model for symmetric definite positive matrices with Euclidean

covariates. Later, [Yuan et al. \(2012\)](#) studied the local polynomial regression in the same setting. [Steinke and Hein \(2009\)](#) consider nonparametric regression between general Riemannian manifolds. [Petersen and Müller \(2017\)](#) developed a novel Fréchet regression approach for complex random objects with euclidean covariates. We believe our work will be a valuable addition to the literature.

2 Geometric Interpretation

We briefly introduce $\text{Sym}_*^+(m)$, the Riemannian manifold consisting of all $m \times m$ symmetric positive definite matrices, while we refer readers to the appendix for more details. A Riemannian manifold is a smooth manifold endowed with an inner product $\langle \cdot, \cdot \rangle_x$ on the tangent space at each point x , such that $\langle \cdot, \cdot \rangle_x$ varies with x smoothly. We consider the Log-Euclidean metric for the symmetric positive definite matrix manifold due to its computational tractability ([Arsigny et al., 2007](#)). Other metrics include the naive Frobenius metric which does not account for the curved nature of symmetric positive definite matrices and the affine invariant metric which is more difficult to compute ([Terras, 2012](#)).

For a manifold \mathcal{M} , we use $T_x\mathcal{M}$ to denote the tangent space at the base point x . It can be shown that the tangent space $T_I\text{Sym}_*^+(m)$ at the identity matrix I is the space of $m \times m$ symmetric matrices, denoted by $\text{Sym}(m)$. For the Log-Euclidean metric, the inner product between $U, V \in \text{Sym}(m)$ on $T_I\text{Sym}_*^+(m)$ at the identity matrix I is defined as $\langle U, V \rangle_I = \text{trace}(UV)$. To define the inner product at a general point, we utilize the concept of differential maps. For a smooth transformation $\varphi : \mathcal{N} \rightarrow \mathcal{M}$ between two manifolds, its differential at x , denoted by φ'_x , is a linear map sending a tangent vector $v \in T_x\mathcal{N}$ to a tangent vector $\varphi'_x(v) \in T_{\varphi(x)}\mathcal{M}$. See [Figure 1](#) for a graphical illustration. When both \mathcal{N} and \mathcal{M} are Euclidean submanifolds, the differential φ'_x is the usual notion of differential of the function φ at x , given by a Jacobian matrix. With this formalism, we consider the smooth map $\log : \text{Sym}_*^+(m) \rightarrow \text{Sym}(m)$, where \log is the matrix logarithm, the inverse map of the matrix exponential. The matrix exponential of a matrix $U \in \text{Sym}(m)$ is defined as $\exp(U) = \sum_{k=0}^{\infty} U^k/k!$. The Riemannian metric at a general point S is then defined as $\langle U, V \rangle_S = \langle \log'_S U, \log'_S V \rangle_I$, where $\log'_S : T_S\text{Sym}_*^+(m) \rightarrow T_S\text{Sym}(m)$ is a linear operator ([Arsigny et al., 2007](#)). The Riemannian exponential map under this metric is given by $\text{Exp}_S U = \exp(\log S + \log'_S U)$, where \exp is the matrix exponential. Riemannian exponential maps are closely related to the intrinsic properties of a manifold, such as the geodesics and the Gauss curvature ([Lee, 1997](#)).

3 Methodology

3.1 A Heterogeneous Matrix-log Mean Model

Suppose we have collected a sequence of matrix-valued observations $Y_1, \dots, Y_n \in \text{Sym}_*^+(m)$. We propose the following matrix-log mean model for investigating the mean changes of the

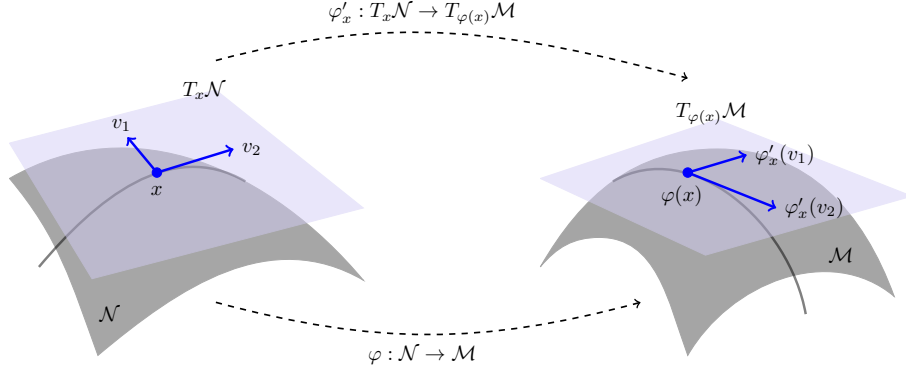


Figure 1: Illustration of smooth map between manifolds and its differential.

data sequence

$$\log Y_i = \log \mu_i + \log'_{\mu_i} \varepsilon_i, \quad (3.1)$$

where $\mu_i \in \text{Sym}_*^+(m)$ is the mean matrix, and $\varepsilon_i \in T_{\mu_i} \text{Sym}_*^+(m)$ is a mean-zero error term in $T_{\mu_i} \text{Sym}_*^+(m)$. Here $\log'_{\mu_i} : T_{\mu_i} \text{Sym}_*^+(m) \rightarrow T_{\log \mu_i} \text{Sym}(m)$ is a linear operator acting on ε_i . The noise term $\log'_{\mu_i} \varepsilon_i$ has mean zero, but the corresponding covariance depends on μ_i . Hence model (3.1) has a heterogeneous noise component.

Interestingly, the heterogeneity of the noise terms makes use of the Riemannian manifold structure introduced in Section 2. Without using the geometric structure, one could simply apply the matrix logarithm first and then model the random SPD matrices Y_i 's as

$$\log Y_i = \log \mu_i + \xi_i,$$

where ξ_i 's are identically distributed random elements. This naive model, first introduced by Chiu et al. (1996), misses the curved structure in the SPD manifold, and thus is less efficient for estimation and inference. Different from theirs, we introduce the location-dependent transformations \log'_{μ_i} in model (3.1) to respect the original manifold structure, because it turns this model into a geodesic/intrinsic mean model. To appreciate this, we take matrix exponential on both sides and find that

$$Y_i = \exp(\log \mu_i + \log'_{\mu_i} \varepsilon_i) = \text{Exp}_{\mu_i} \varepsilon_i.$$

It can be shown that μ_i is the minimizer to the following optimization program

$$\mu_i = \underset{S \in \text{Sym}_*^+(m)}{\text{argmin}} \mathbb{E} g^2(S, Y_i),$$

where $g(S, Y_i)$ is the geodesic distance between S and Y_i in $\text{Sym}_*^+(m)$. Therefore, model (3.1) serves as an exact counterpart of the Euclidean mean model $Y = \mu + \varepsilon \in \mathbb{R}^d$, where μ minimizes $\mathbb{E} \|Y - a\|_2^2$ over $a \in \mathbb{R}^d$.

Remark 1. We emphasize that the idea of using a matrix logarithm to model SPD matrices was first explored by [Leonard and Hsu \(1992\)](#) and [Chiu et al. \(1996\)](#). However, their approach does not take the manifold structure into account. From the modeling perspective, our key contribution is that we establish a parametric model for SPD matrices that respects the original manifold structure.

Model (3.1) provides a natural way to investigate change-point detection problems for SPD manifold-valued data. For this purpose, we further assume that there exist $\mathcal{J} = \{\tau_j : j = 1, \dots, J\}$ and $1 \leq \tau_1 < \dots < \tau_J \leq n - 1$ such that $\mu_\tau \neq \mu_{\tau+1}$ if $\tau \in \mathcal{J}$ and $\mu_\tau = \mu_{\tau+1}$ otherwise. Elements in \mathcal{J} are called change points. Our goal is to detect \mathcal{J} based on the data sequence Y_1, \dots, Y_n .

3.2 Computational Details

Computationally, it is more convenient to work with a basis of the space $\text{Sym}(m)$ which is a $d = m(m+1)/2$ dimensional Hilbert space under the Frobenius inner product. The Frobenius inner product between $A = (a_{ij})$ and $B = (b_{ij})$ is defined as $\langle A, B \rangle_{\text{F}} = \sum_{i,j=1}^m a_{ij}b_{ij}$. Let $\phi = \{\phi_k : 1 \leq k \leq d\}$ be an orthonormal basis of $\text{Sym}(m)$ under this inner product. Then, for any $A \in \text{Sym}(m)$, we can write $A = \sum_{k=1}^d c_k \phi_k$ with $c_k = \langle A, \phi_k \rangle_{\text{F}}$, and identify it with its coefficient vector $(c_1, \dots, c_d)^{\text{T}}$, denoted by \vec{A} .

In this paper, we adopt the basis constructed in the following. Let B_{ij} be the matrix of zeros except the (i, j) and (j, i) entries, which are set to 1 if $i = j$, and $1/\sqrt{2}$ otherwise. Since $B_{ij} = B_{ji}$, we consider basis matrices B_{ij} 's with $i \geq j$. It can be checked that $\|B_{ij}\|_{\text{F}} = 1$ and $\langle B_{ij}, B_{k\ell} \rangle_{\text{F}} = 0$ if $i \neq k$ or $j \neq \ell$, where $\|\cdot\|_{\text{F}}$ denotes the Frobenius norm. Let $\phi_{i(i-1)/2+j} = B_{ij}$, and then $\{B_{ij} : 1 \leq j \leq i \leq m\}$ form an orthonormal basis for $\text{Sym}(m)$. We use this basis in our computation. Note that the results presented in the paper are identical for all bases.

To compute the matrix logarithm $\log Y$ for $Y \in \text{Sym}_{\star}^+(m)$, we first find a unitary matrix P such that $Y = P\Lambda P^{-1}$ for a diagonal matrix $\Lambda = \text{diag}(\lambda_1, \dots, \lambda_m)$. The matrices P and Λ can be computed by eigendecomposition or singular value decomposition (SVD). Then $\log Y = P \log(\Lambda) P^{-1}$ with $\log \Lambda = \text{diag}(\log \lambda_1, \dots, \log \lambda_m)$.

To compute the matrix representation of the linear differential operator \log'_{μ} for a given symmetric positive definite matrix μ with respect to the basis ϕ , we first note that $\log'_{\mu} = (\exp'_{\log \mu})^{-1}$ ([Arsigny et al., 2007](#)). Therefore, once we have the matrix representation Q of the linear operator $\exp'_{\log \mu}$ with respect to the basis ϕ , then Q^{-1} will be the matrix representation of \log'_{μ} , noting that the non-singularity of $\exp'_{\log \mu}$ everywhere implies the invertibility of Q . If $\zeta_j \in \mathbb{R}^d$ is the coefficient vector (viewed as a column vector) of $\exp'_{\log \mu} \phi_j$ with respect to a chosen basis, then it is seen that the Q is given by the matrix $Q = [\zeta_1 \dots \zeta_d]$ concatenated by column vectors ζ_j . Therefore, the problem boils down to

the computation of

$$\exp'_{\log \mu} \phi_j = \sum_{k=1}^{\infty} \frac{1}{k!} \sum_{\ell=0}^{k-1} (\log \mu)^{k-\ell-1} \cdot \phi_j \cdot (\log \mu)^\ell.$$

Numerically, the above series is truncated at a sufficiently large K . Note that when $\mu = I_m$, we have specially $\exp'_{\log \mu} = I_m$.

3.3 A Local Scan Procedure

Roughly speaking, an ideal statistic for detecting change patterns, or change points, at a position x should directly relate to the possibility that x is a change point. The statistic at the position x we proposed is a locally weighted average of the transformed Y_i 's near x :

$$G(x, h) = \sum_{i=1}^n w_i(h) \overrightarrow{\log Y_i},$$

where $w_i(h) = 1/h$ if $1 - h \leq i - x \leq 0$, $w_i(h) = -1/h$ if $1 \leq i - x \leq h$, and $w_i(h) = 0$ otherwise. We remind the readers that \overrightarrow{A} denotes the coefficient vector of the matrix A with respect to a basis ϕ . The $G(x, h)$ defined above is constructed based on data points within a local window of size $2h$ around the point x . The intuition is that, if there is no change point within the window $(x - h, x + h)$, then $G(x, h)$ has mean zero and $\|G(x, h)\|_2$ is close to zero. Otherwise, if $\|G(x, h)\|_2$ is large, then x is likely to be a change point. In particular, points that locally maximize $\|G(\cdot, h)\|_2$ have a high chance of being a change point. We say that x is a h local maximizer if $\|G(x, h)\|_2 \geq \|G(j, h)\|_2$ for all $j \in \{x - h, \dots, x + h\}$. The set of h local maximizers is denoted by $\mathcal{L}(h)$. Suppose $\|G(j_1, h)\|_2 \geq \|G(j_2, h)\|_2 \geq \dots \geq \|G(j_\ell, h)\|_2$, where ℓ is the number of elements in $\mathcal{L}(h)$. For a given threshold $\rho > 0$, we then estimate \mathcal{J} by $\hat{\mathcal{J}} = \{\tau \in \mathcal{L}(h) : \|G(\tau, h)\|_2^2 \geq \rho\}$, and J is estimated by the cardinality of $\hat{\mathcal{J}}$.

However, the above procedure for estimating J depends on the unknown parameter ρ . In practice, we propose a data-driven alternative based on the K -fold cross validation to select the number of change points. Suppose that $j_{(1)}, \dots, j_{(k)}$ are change points, which divided all time points into $k + 1$ segments. Within each segment, time points are randomly split into K partitions. The sample mean of a segment is estimated by using data from any $K - 1$ partitions within that segment, and the validation error is evaluated on the rest one partition. The cross validation error of the segment is defined to be the sum of validation errors from the K partitions, while the total cross-validation error is the sum of cross-validation errors across all $k + 1$ segments. Formally, the total cross-validation error is defined as

$$CV(k) = \sum_{q=1}^{k+1} \sum_{p=1}^K \sum_{i \in \mathcal{P}_{q,p}} (\widehat{\log \mu_{q,p}} - \overrightarrow{\log Y_i})^\top (\widehat{\log \mu_{q,p}} - \overrightarrow{\log Y_i}),$$

where $\mathcal{P}_{q,p}$ is the p th partition of the q th segment, and $\widehat{\log \mu_{q,p}} = |\mathcal{P}_{q,-p}|^{-1} \sum_{i \in \mathcal{P}_{q,-p}} \overrightarrow{\log Y_i}$. Here $\mathcal{P}_{q,-p}$ denotes the time points in the q th segment but not in the partition $\mathcal{P}_{q,p}$ and

$|\mathcal{P}_{q,-p}|$ the cardinality of the set $\mathcal{P}_{q,-p}$. The integer that minimizes $CV(\cdot)$ is chosen as an estimate of J . We then estimate the locations of change points using the proposed scan statistics.

4 Asymptotic Theory

A random vector $\xi \in \mathbb{R}^d$ is called a subgaussian vector with parameter (ν, σ) if $\eta \geq 0$, $\nu \in \mathbb{R}^d$ and for all $a \in \mathbb{R}^d$,

$$E[\exp(a^\top(\xi - \nu))] \leq \exp(\|a\|^2 \sigma^2 / 2).$$

We say that a random element in $\text{Sym}(m)$ is subgaussian if its coefficient vector with respect to the orthonormal basis ϕ is subgaussian. One can easily check that this definition is independent of the choice of the orthonormal basis of $\text{Sym}(m)$. Below we shall assume $\log'_{\mu_i} \varepsilon_i$ is subgaussian with parameter $(0, \sigma_i)$. This σ_i might depend on μ_i and thus the linear operator \log'_{μ_i} and its matrix representation Σ_i . For example, one might conceive of i.i.d. subgaussian random elements $\varepsilon_1, \dots, \varepsilon_n$ and applying Σ_i to ε_i , where different transformations result in different distributions of $\log'_{\mu_i} \varepsilon_i$. Although subgaussianity is well preserved by linear transformations, the subgaussian parameter might differ after transformation. For example, one can show that, if ε_i is subgaussian with a parameter θ , then $\log'_{\mu_i} \varepsilon_i$ is subgaussian, but with a parameter $\theta \sqrt{\|\Sigma_i \Sigma_i^\top\|}$. In this case, σ_i might quantify the magnitude, measured by $\sqrt{\|\Sigma_i \Sigma_i^\top\|}$, of the transformation \log'_{μ_i} .

To derive the sure coverage property of the proposed procedure, we define $\delta = \inf\{\|\delta_\tau\|_2 : \tau \in \mathcal{J}\}$, $\sigma = \max\{\sigma_1, \dots, \sigma_n\}$, and $L = \inf_{1 \leq j \leq J}(\tau_j - \tau_{j-1})$, where we conventionally denote $\tau_0 = 0$ and $\tau_{J+1} = n$. We need the following assumption.

Assumption 1. The quantities δ , L , and σ satisfy that $\delta^2 L \geq 16\sigma^2(d + 2\sqrt{d} + 2 \log n + 2 \log \log n)$.

Here, σ characterizes the variability of $\log'_{\mu_i} \varepsilon_i$'s over all time points. The quantity δ characterizes the strength of the weakest signal of change points, while L indicates the separability of change points. Intuitively, when δ and L are small, no method would succeed in recovering all change points. Recall that $d = m(m+1)/2$ denotes the dimension of the space $\text{Sym}_*^+(m)$. It is seen that detection of change points becomes harder for higher dimensional matrices, i.e., a larger m , since stronger signal (larger δ) or better separation of change points (larger L) is required to make the inequality in the above assumption hold.

Now we establish the sure coverage property of the proposed procedure, that is, the union of the intervals selected by our procedure recovers all change points with probability going to 1. A nonasymptotic probability bound is also derived, with explicit dependence on the sample size n . We use $\mathcal{J} \subset \widehat{\mathcal{J}} \pm h$ to denote that $\tau_j \in (\widehat{\tau}_j - h, \widehat{\tau}_j + h)$ for all $j = 1, \dots, J$. We are ready to state the main theorem of this paper, whose proof is deferred to the appendix.

Theorem 4.1. Suppose that Assumption 1 holds. If $\rho = \delta^2/4$ and $h = L/2$, then

$$\Pr(\widehat{J} = J, \mathcal{J} \subset \widehat{\mathcal{J}} \pm h) \rightarrow 1, \text{ as } n \rightarrow \infty.$$

Remark 2. We emphasize here that the dimension d does not need to be assumed to be fixed and could potentially diverge to infinity as long as Assumption 1 holds.

5 Simulation Studies

In this section, we examine the empirical performance of our method. We generate data according to model (3.1). In the first example, we consider different combinations of n, m, J such that $(n, m, J) = (100, 6, 2), (200, 6, 2), (200, 6, 4), (400, 6, 4)$ respectively. When $J = 2$, we set $\mu_1 = \dots = \mu_{n/4} = I_m, \mu_{n/4+1} = \dots = \mu_{3n/4} = 2I_m$ and $\mu_{3n/4+1} = \dots = \mu_n = 5I_m$. When $J = 4$, we set $\mu_{kn/5+1} = \dots = \mu_{(k+1)n/5} = A_k$ for $k = 0, \dots, 4$, where $A_1 = I_m, A_2 = \text{diag}(I_{m/2}, 3I_{m/2}), A_3 = 3I_m, A_4 = \text{diag}(3I_{m/2}, 10I_{m/2})$, and $A_5 = 10I_m$. For the symmetric random noise, we first sample the coefficient vector from distribution $N(0, I_d)$, then combine it with the basis ϕ to generate the noise ε_i . Our second example is concerned with a larger m by setting that $(n, m, J) = (100, 10, 2), (200, 10, 2), (200, 10, 4), (400, 10, 4)$.

Choosing the optimal bandwidth is usually a difficult task for change point problems, see, for example, [Niu and Zhang \(2012\)](#) for a detailed discussion. Intuitively, when there is only one change point in the interval $(x - h, x + h)$, the larger h is, the more powerful the scan statistic is. But when the bandwidth gets too large, the interval might contain multiple change points. Therefore we need to choose bandwidth carefully. In our simulations, we found that the performance of the procedure is relatively robust to the choice of the bandwidth as long as the bandwidth is not too large, and $h = 20$ works relatively well in our case. We use the proposed cross validation technique to select the number of change points. We run 100 repetitions of Monte Carlo studies. For each run, we calculate the estimated number of change points and the locations of the change points. We report the frequencies of the three cases: $\widehat{J} < J, \widehat{J} = J$ and $\widehat{J} > J$, the mean of the number of change points detected, and the sure coverage probability for each of the change point. We also compare two methods that are frequently used in practice. The first one vectorizes the response Y_i without considering any manifold structure, which results in a m^2 -dimensional vector. We denote this method as ‘‘Vector’’. The other one also adopts the vectorization idea, but additionally takes the symmetric information into account, yielding a $m(m+1)/2$ -dimensional vector. We use ‘‘Symmetric’’ to denote this method. The results are summarized in [Tables 1 and 2](#).

As indicated by the results, our proposed method performs better than the comparison methods in terms of the percentage of correctively recovering the number of change points, in all cases. Additionally, when $J = 2$, all the methods presented here can detect the second change point very well. But for the first one, our method achieves a higher sure coverage

Table 1: The frequency of the number of change points when $\hat{J} < J$, $\hat{J} = J$ and $\hat{J} > J$, the mean (s.e.) of the number of change points, and SCP of each change-point are reported. The results are based on 100 replications.

(n, m, J)	Method	$\hat{J} < J$	$\hat{J} = J$	$\hat{J} > J$	Mean	SCP 1	SCP 2	SCP 3	SCP 4
(100, 6, 2)	Proposed	0.01	0.99	0	1.99(0.01)	0.99	1	NA	NA
	Vector	0.32	0.62	0.06	1.74(0.06)	0.67	0.99	NA	NA
	Symmetric	0.13	0.82	0.05	1.92(0.04)	0.83	1	NA	NA
(200, 6, 2)	Proposed	0	0.95	0.05	2.05(0.02)	1	1	NA	NA
	Vector	0.64	0.22	0.14	1.56(0.09)	0.17	0.99	NA	NA
	Symmetric	0.65	0.17	0.18	1.62(0.1)	0.22	1	NA	NA
(200, 6, 4)	Proposed	0.03	0.94	0.03	4(0.02)	1	0.99	0.99	0.99
	Vector	0.56	0.27	0.17	3.08(0.14)	0.47	0.48	0.93	0.89
	Symmetric	0.45	0.3	0.25	3.39(0.15)	0.58	0.62	0.95	0.89
(400, 6, 4)	Proposed	0	0.92	0.08	4.09(0.03)	1	1	1	1
	Vector	0.6	0.23	0.17	3.28(0.18)	0.05	0.1	0.73	0.89
	Symmetric	0.55	0.25	0.2	3.59(0.2)	0.1	0.15	0.85	0.88

s.e., standard error; SCP, sure coverage probability; NA, not available.

probability. When $J = 4$, our method achieves a higher sure coverage probability for all the change points. These results suggest the importance of considering the geometric structure of the Riemannian data, at least, in change point detection problems.

6 An Application to the Human Connectome Project

We apply the proposed methodology to the social cognition task related fMRI data from Human Connectome Project Dataset, which includes behavioral and 3T MR imaging data from 970 healthy adult participants collected from 2012 to spring 2015. We focus on the 850 subjects out of the 970 which have the social cognition task related fMRI data. Participants were presented with short video clips (20 seconds) of objects (squares, circles, triangles) that either interacted in some way, or moved randomly on the screen (Castelli et al., 2000; Wheatley et al., 2007). There were 5 video blocks (2 Mental and 3 Random in one run, 3 Mental and 2 Random in the other run) in the task run.

We use the ‘‘Desikan-Killiany’’ atlas (Desikan et al., 2006) to divide the brain into 68 regions of interest. Figure 2(a) shows the ‘‘Desikan-Killiany’’ parcellation of the cortical surface in the left and right hemisphere. We pick eight possible regions that are related to the social task, that are the left and right part of superior temporal, inferior parietal, temporal pole and precuneus (Green et al., 2015). These eight regions of interest are highlighted in yellow in Figure 2(b). For each subject, the fMRI data are recorded on 274 evenly spaced time points, one per 0.72 seconds. We use a moving local window of size 100 to calculate the cross covariance between these eight regions, which results in 175 cross covariance matrices with dimensions 8×8 . We then apply the proposed method to detect change points in this sequence of cross covariance matrices with bandwidth h set to be 20.

Table 2: The frequency of the number of change points when $\hat{J} < J$, $\hat{J} = J$ and $\hat{J} > J$, the mean (s.e.) of the number of change points, and the SCP of each change-point are reported. The results are based on 100 replications.

(n, m, J)	Method	$\hat{J} < J$	$\hat{J} = J$	$\hat{J} > J$	Mean	SCP 1	SCP 2	SCP 3	SCP 4
(100, 10, 2)	Proposed	0.01	0.99	0	1.99(0.01)	0.99	1	NA	NA
	Vector	0.61	0.38	0.01	1.4(0.05)	0.37	1	NA	NA
	Symmetric	0.27	0.69	0.04	1.77(0.05)	0.72	1	NA	NA
(200, 10, 2)	Proposed	0	0.98	0.02	2.02(0.01)	1	1	NA	NA
	Vector	0.67	0.17	0.16	1.51(0.08)	0.17	0.97	NA	NA
	Symmetric	0.74	0.11	0.15	1.45(0.09)	0.21	1	NA	NA
(200, 10, 4)	Proposed	0.04	0.96	0	3.96(0.02)	1	0.96	1	1
	Vector	0.51	0.31	0.18	3.28(0.12)	0.33	0.57	0.94	0.96
	Symmetric	0.44	0.36	0.2	3.38(0.13)	0.51	0.65	0.96	0.96
(400, 10, 4)	Proposed	0	1	0	4(0)	1	1	1	1
	Vector	0.64	0.21	0.15	2.95(0.19)	0.03	0.08	0.55	0.89
	Symmetric	0.51	0.25	0.24	3.66(0.22)	0.1	0.17	0.76	0.93

s.e., standard error; SCP, sure coverage probability; NA, not available.

We apply the method to all the subjects, and report the locations of change points detected for each subject. In Table 3, we have summarized the count and percentage of the number of change points detected for all the subjects. The mean number of change points detected among all the subjects is 3.66(0.03). This result matches the physiology well since there are 5 video blocks in the task design, with changes at the time points 35, 70, 105 and 140 respectively. To further validate the proposed methodology, we pick up all those subjects with four change points, and calculate the mean locations respectively. The means are 39.6, 72.0, 106.7, 138.5, which are fairly close to the task block changes. A more interesting observation is that the lags (4.6s, 2.0s, 1.7s and -1.5s) are becoming shorter and shorter: the last time point even precedes the designed time point. This, to our understanding, witnesses the powerfulness of human brains for learning the change patterns.

Table 3: The count and percentage of the number of change points detected for social task related fMRI data.

Number of Change Points	1	2	3	4	5
Count	1	55	291	387	116
Percentage	0.12%	6.47%	34.24%	45.53%	13.65%

7 Discussion

In this paper we propose an additive matrix-log mean model with a heterogeneous noise for modeling random symmetric positive definite matrices that lie in a Riemannian manifold. The heterogeneous noise part takes account the manifold structure of the original symmetric positive definite matrices. Built upon this model, we then propose a scan statistic to perform

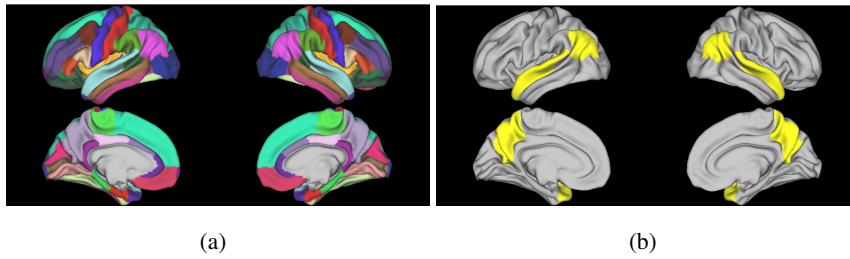


Figure 2: Panel (a): the “Desikan-Killiany” parcellation of the cortical surface in left and right hemisphere. Panel (b): the eight regions of interest.

multiple change point detection. Theoretical studies and numerical examples lend further support to our proposed methodology.

Our proposed methodology relies on the assumption that the collected samples Y_i 's are independent. Independence is an ideal assumption that may be violated in some settings. However, this assumption allows us to conduct theoretical analysis, which also produce results that could be useful when the assumption is violated. We will pursue the change-point detection problems under dependence for Riemannian data in future work.

References

- ARSIGNY, V., FILLARD, P., PENNEC, X. and AYACHE, N. (2007). Geometric means in a novel vector space structure on symmetric positive-definite matrices. *SIAM Journal of Matrix Analysis and Applications* **29** 328–347.
- CARLSTEIN, E. G., MÜLLER, H.-G. and SIEGMUND, D. (1994). Change-point problems. Institute of Mathematical Statistics.
- CASTELLI, F., HAPPÉ, F., FRITH, U. and FRITH, C. (2000). Movement and mind: a functional imaging study of perception and interpretation of complex intentional movement patterns. *NeuroImage* **12** 314–325.
- CHEN, H. and ZHANG, N. (2015). Graph-based change-point detection. *The Annals of Statistics* **43** 139–176.
- CHIU, T. Y., LEONARD, T. and TSUI, K.-W. (1996). The matrix-logarithmic covariance model. *Journal of the American Statistical Association* **91** 198–210.
- DANIELS, M. J. and POURAHMADI, M. (2002). Bayesian analysis of covariance matrices and dynamic models for longitudinal data. *Biometrika* **89** 553–566.
- DESIKAN, R. S., SÉGONNE, F., FISCHL, B., QUINN, B. T., DICKERSON, B. C., BLACKER, D., BUCKNER, R. L., DALE, A. M., MAGUIRE, R. P. and HYMAN, B. T. (2006). An automated labeling system for subdividing the human cerebral cortex on MRI scans into gyral based regions of interest. *NeuroImage* **31** 968–980.

- DRYDEN, I. L., KOLOYDENKO, A. and ZHOU, D. (2009). Non-Euclidean statistics for covariance matrices, with applications to diffusion tensor imaging. *The Annals of Applied Statistics* **3** 1102–1123.
- FLETCHER, P. T. (2013). Geodesic regression and the theory of least squares on Riemannian manifolds. *International Journal of Computer Vision* **105** 171–185.
- FRISTON, K. J. (2011). Functional and effective connectivity: a review. *Brain Connectivity* **1** 13–36.
- GREEN, M. F., HORAN, W. P. and LEE, J. (2015). Social cognition in schizophrenia. *Nature Reviews. Neuroscience* **16** 620–631.
- HSU, D., KAKADE, S. and ZHANG, T. (2012). A tail inequality for quadratic forms of subgaussian random vectors. *Electronic Communications in Probability* **17** 1–6.
- HUTCHISON, R. M., WOMELSDORF, T., ALLEN, E. A., BANDETTINI, P. A., CALHOUN, V. D., CORBETTA, M., DELLA PENNA, S., DUYN, J. H., GLOVER, G. H. and GONZALEZ-CASTILLO, J. (2013). Dynamic functional connectivity: promise, issues, and interpretations. *NeuroImage* **80** 360–378.
- JAMES, B., JAMES, K. L. and SIEGMUND, D. (1987). Tests for a change-point. *Biometrika* **74** 71–83.
- LEE, J. M. (1997). *Riemannian Manifolds: An Introduction to Curvature*. Springer-Verlag, New York.
- LEONARD, T. and HSU, J. S. (1992). Bayesian inference for a covariance matrix. *The Annals of Statistics* 1669–1696.
- NIU, Y. S. and ZHANG, H. (2012). The screening and ranking algorithm to detect DNA copy number variations. *The Annals of Applied Statistics* **6** 1306–1326.
- OLSHEN, A. B., VENKATRAMAN, E., LUCITO, R. and WIGLER, M. (2004). Circular binary segmentation for the analysis of array-based dna copy number data. *Biostatistics* **5** 557–572.
- PETERSEN, A. and MÜLLER, H.-G. (2017). Fréchet regression for random objects with Euclidean predictors. *The Annals of Statistics* to appear.
- SCHWARTZMAN, A. (2006). *Random ellipsoids and false discovery rates: Statistics for diffusion tensor imaging data*. Ph.D. thesis, Stanford University.
- STEINKE, F. and HEIN, M. (2009). Non-parametric regression between manifolds. In *Advances in Neural Information Processing Systems*.

- TERRAS, A. (2012). *Harmonic analysis on symmetric spaces and applications II*. Springer Science & Business Media.
- TIBSHIRANI, R. and WANG, P. (2007). Spatial smoothing and hot spot detection for cgh data using the fused lasso. *Biostatistics* **9** 18–29.
- WHEATLEY, T., MILLEVILLE, S. C. and MARTIN, A. (2007). Understanding animate agents: distinct roles for the social network and mirror system. *Psychological Science* **18** 469–474.
- XU, Y. and LINDQUIST, M. A. (2015). Dynamic connectivity detection: an algorithm for determining functional connectivity change points in fmri data. *Frontiers in Neuroscience* **9**.
- YAO, Y.-C. (1988). Estimating the number of change-points via Schwarz' criterion. *Statistics & Probability Letters* **6** 181–189.
- YUAN, Y., ZHU, H., LIN, W. and MARRON, J. S. (2012). Local polynomial regression for symmetric positive definite matrices. *Journal of the Royal Statistical Society: Series B* **74** 697–719.
- ZHANG, N. R. and SIEGMUND, D. O. (2007). A modified bayes information criterion with applications to the analysis of comparative genomic hybridization data. *Biometrics* **63** 22–32.
- ZHU, H., CHEN, Y., IBRAHIM, J. G., LI, Y., HALL, C. and LIN, W. (2009). Intrinsic regression models for positive-definite matrices with applications to diffusion tensor imaging. *Journal of the American Statistical Association* **104** 1203–1212.

Appendix

S.1 Preliminary

In this section, we further discuss the smooth and Riemannian manifold. For a comprehensive treatment on these subjects, readers are referred to the introductory book by [Lee \(1997\)](#).

A smooth manifold \mathcal{M} is a differentiable manifold with all transition maps being C^∞ -differentiable. Associated with each point x on the manifold \mathcal{M} , there exists a linear space $T_x\mathcal{M}$ called the tangent space at the base point x . Each element in the tangent space is called a tangent vector. For a manifold that is a submanifold of a Euclidean space, the tangent space at a point can be geometrically visualized as the hyperplane tangent to that point, while tangent vectors are visualized as Euclidean vectors tangent to the manifold at that point; see [Figure S.3](#) for an illustration. It is emphasized that tangent vectors at different base points are different, despite that the vectors might point to the same direction. Thus, a tangent vector always implicitly comes with a base point. For Euclidean submanifolds, a tangent vector v at a point x can also be algebraically interpreted as a directional derivative D_v at x , such that $D_v f = v^T \nabla f(x)$ for all $f \in C^\infty(\mathcal{M})$ with $C^\infty(\mathcal{M})$ denoting the collection of real-valued smooth functions defined on the manifold \mathcal{M} . Observe that D_v is a derivation at x , which satisfies the Leibniz rule,

$$D_v(fg) = g(x)(D_v f) + f(x)(D_v g),$$

for any $f, g \in C^\infty(\mathcal{M})$ and $v \in T_x\mathcal{M}$, where fg denotes the pointwise product of functions. This allows one to generalize the concept of tangent vector as directional derivative to non-Euclidean manifolds, by defining tangent vectors at x as derivations at x , and tangent space at x as the space of derivations at x . A convenient way to perceive the derivation represented by a tangent vector v is to treat $D_v : C^\infty(\mathcal{M}) \rightarrow \mathbb{R}$ as a linear functional that maps $C^\infty(\mathcal{M})$ into \mathbb{R} .

For a smooth transformation $\varphi : \mathcal{N} \rightarrow \mathcal{M}$ that maps points on a manifold \mathcal{N} to points on the manifold \mathcal{M} , its *differential* at x , denoted by φ'_x , is a linear map sending a tangent vector $v \in T_x\mathcal{N}$ to a tangent vector $\varphi'_x(v) \in T_{\varphi(x)}\mathcal{M}$, such that the derivation $D_{\varphi'_x(v)}$ corresponding to the tangent vector $\varphi'_x(v)$ at the point $\varphi(x) \in \mathcal{M}$ is depicted by

$$D_{\varphi'_x(v)} : C^\infty(\mathcal{M}) \rightarrow \mathbb{R}, \quad \text{s.t. } \forall f \in C^\infty(\mathcal{M}) : D_{\varphi'_x(v)} f = D_v(f \circ \varphi),$$

where $f \circ g$ denotes the composition of functions. When both \mathcal{N} and \mathcal{M} are Euclidean submanifolds, the differential φ'_x is the usual notion of differential of the function φ at x , given by a Jacobian matrix. Specially, when \mathcal{N} is an interval (a, b) of the real line, the tangent space at each $t \in (a, b)$ is the whole real line \mathbb{R} . In this case, φ is often called a (parameterized) smooth curve on \mathcal{M} , and $\varphi'_t(1)$ is denoted by $\varphi'(t)$ which is the derivative of the curve at time t . Here, to properly decode the notation $\varphi'_t(1)$, recall that φ'_t is a map

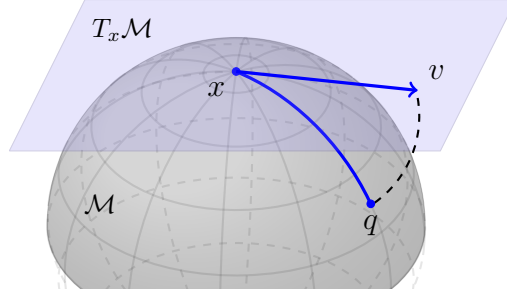


Figure S.3: Geometric illustration of tangent vector, tangent space, curve and exponential map. $\gamma(t)$ with $\gamma(0) = x$ and $\gamma(1) = q$ is a smooth curve on \mathcal{M} . v is a tangent vector at x and also tangent to the curve γ at $t = 0$, i.e. $v = \gamma'(0)$. If in addition $\gamma(t)$ is a geodesic, then $q = \gamma(1) = \text{Exp}_x(v)$.

sending a tangent vector of a manifold to a tangent vector of another manifold, and for the special manifold (a, b) , the real number 1 can be viewed as a tangent vector at $t \in (a, b)$. Geometrically and intuitively, $\varphi'(t)$ is a vector tangent to the curve φ at time t , as illustrated in Figure S.3.

A Riemannian manifold is a smooth manifold endowed with an inner product $\langle \cdot, \cdot \rangle_x$ on the tangent space at each point x , such that $\langle \cdot, \cdot \rangle_x$ varies with x smoothly. The collection of such inner products is often called the Riemannian metric tensor, or simply Riemannian metric. One can show that, the metric tensor induces a distance function that turns the manifold into a metric space. A geodesic is a smooth curve on the manifold such that for any sufficiently small segment, the segment is the unique smooth curve with the minimal length among all smooth curves connecting the two endpoints of the segment. Every smooth curve on the manifold can be parameterized by a smooth map γ from an interval in \mathbb{R} to the manifold. For any $u \in T_x \mathcal{M}$, there exists a unique geodesic γ such that $\gamma'(0) = u$ and $\gamma(0) = x$. Then the exponential map at x , denoted by Exp_x , is defined by $\text{Exp}_x(u) = \gamma(1)$. For example, one can verify that for the unit circle $\mathbb{S}^1 \equiv \{(z_1, z_2) \in \mathbb{R}^2 : z_1^2 + z_2^2 = 1\}$, for $x \in \mathbb{S}^1$ and $v \in T_x \mathbb{S}^1$, the defining geodesic for the Riemannian exponential map Exp_x is $\gamma(t) = \cos(t\|u\|_2)x + \sin(t\|u\|_2)u/\|u\|_2$, as $\gamma(0) = x$ and $\gamma'(0) = u$. Thus, $\text{Exp}_x(u) = \gamma(1) = \cos(\|u\|_2)x + \sin(\|u\|_2)u/\|u\|_2$. A graphical illustration of the Exp map is given in Figure S.3.

For the Log-Euclidean metric, at the identity matrix I , it is defined as $\langle U, V \rangle_I = \text{trace}(UV)$ for $U, V \in \text{Sym}(m) = T_I \text{Sym}_*^+(m)$, the Frobenius inner product on $\text{Sym}(m)$. In order to define metric at other points, the following group structure is considered. Define $S_1 \odot S_2 = \exp(\log S_1 + \log S_2)$, where \exp and \log are the matrix exponential and logarithm respectively. The operation \odot turns $\text{Sym}_*^+(m)$ into a group. Now we define the left-translation operator $\mathcal{L}_S Q = S \odot Q$ for $S, Q \in \text{Sym}_*^+(m)$. As shown in [Arsigny et al. \(2007\)](#), \mathcal{L}_S is a smooth map from \mathcal{M} to itself. Thus, its differential $(\mathcal{L}_S)'_Q$ at Q is a linear

map that sends tangent vectors at S to tangent vectors at $S \odot Q$. For instance, the linear operator $\mathcal{I}_S = (\mathcal{L}_{S^{-1}})'_S$ maps tangent vectors at S to tangent vectors at the identity. Given this property, we can “translate” the metric at the identity matrix to all points by the left-translation operator \mathcal{L} . More specifically, the Log-Euclidean metric at any $S \in \text{Sym}_*^+(m)$ is defined by $\langle U, V \rangle_S = \langle \mathcal{I}_S U, \mathcal{I}_S V \rangle_I = \langle \log'_S U, \log'_S V \rangle_I$ for all $U, V \in \text{Sym}(m)$, where the last identity is due to $(\mathcal{L}_{S^{-1}})'_S = \log'_S$ (Arsigny et al., 2007). The Riemannian exponential map under this metric is given by $\text{Exp}_S U = \exp(\log S + \log'_S U)$.

S.2 Proofs

Lemma S.1. Let $\mathcal{A}_n(h, \rho) = \bigcap_{x \in \mathcal{F}} \{\|G(x, h)\|_2^2 \leq \rho\}$, $\mathcal{B}_n(h, \rho) = \bigcap_{\tau \in \mathcal{J}} \{\|G(\tau, h)\|_2^2 \geq \rho\}$ and $\mathcal{E}_n(h, \rho) = \mathcal{A}_n(h, \rho) \cap \mathcal{B}_n(h, \rho)$, where \mathcal{F} denotes the collection of flat points, i.e., $x \in \mathcal{F}$ if and only if $\mu_j = \mu_x$ for all $j \in \{x - h + 1, \dots, x + h\}$. Then $\mathcal{J} \subset \hat{\mathcal{J}} \pm h$ holds under the event $\mathcal{E}_n(h, \rho)$.

Proof of Lemma S.1. The proof can be found in Lemma 3 of Niu and Zhang (2012). \square

Proof of Theorem 4.1. We first note the following facts about subgaussian random vectors that will be used in the sequel.

- If ξ_1, \dots, ξ_n are independent and subgaussian with parameters $(\mu_1, \eta_1), \dots, (\mu_n, \eta_n)$, respectively, then $\sum_i \xi_i$ is a subgaussian random vector with parameters $\sum_i \mu_i$ and $\{\sum_i \eta_i^2\}^{1/2}$.
- If $\xi \in \mathbb{R}^d$ is a subgaussian random vector with a parameter (μ, η) and A is a $d \times d$ matrix, then $A\xi$ is a subgaussian random vector with parameters $A\mu$ and $\eta\sqrt{\|AA^\top\|}$.

A point x is called a h -flat point (or simply flat point if h is clear from the context) if $\mu_j = \mu_x$ for all $j \in \{x - h, \dots, x + h\}$. For a flat point x , $G(x, h) = \sum_{i=x-h}^x h^{-1} \Sigma_i \vec{\varepsilon}_i - \sum_{i=x+1}^{x+h} h^{-1} \Sigma_i \vec{\varepsilon}_i$ has mean zero and also is a subgaussian random vector with parameters 0 and $\sqrt{2h^{-2} \sum_i \sigma_i^2} \leq \sigma\sqrt{2/h}$. Here, we recall that $\Sigma_i \vec{\varepsilon}_i$ is subgaussian with the parameter $(0, \sigma_i)$. For a change-point τ , similarly, $G(\tau, h)$ is subgaussian with parameter $(\delta_\tau, \sigma\sqrt{2/h})$.

Let $t_n = \log n + \log \log n$ and $a_n = 2\sigma^2 h^{-1}(d + 2\sqrt{d} + 2t_n)$. For a flat point x , we first observe that

$$\Pr\{\|G(x, h)\|_2^2 > a_n\} \leq e^{-t_n} = \frac{1}{n \log n}$$

according to Theorem 1 of Hsu et al. (2012). According to Assumption 1 and the choice of ρ and L , we have $\rho \geq a_n$ and thus

$$\Pr\{\|G(x, h)\|_2^2 > \rho\} \leq \Pr\{\|G(x, h)\|_2^2 > a_n\} \leq \frac{1}{n \log n}.$$

Similarly, from Assumption 1 we deduce that $\|\delta_\tau\|_2 \geq \delta \geq 2\sqrt{a_n}$ and $\sqrt{\rho} \leq \|\delta_\tau\|_2 - \sqrt{a_n}$. Thus, for a change point τ ,

$$\begin{aligned} \Pr\{\|G(\tau, h)\|_2 < \sqrt{\rho}\} &\leq \Pr\{\|G(\tau, h)\|_2 < \|\delta_\tau\|_2 - \sqrt{a_n}\} \\ &\leq \Pr\{|\|G(\tau, h)\|_2 - \|\delta_\tau\|_2| > \sqrt{a_n}\} \\ &\leq \Pr\{\|G(\tau, h) - \delta_\tau\|_2^2 > a_n\} \\ &\leq \frac{1}{n \log n}, \end{aligned}$$

or equivalently,

$$\Pr\{\|G(\tau, h)\|_2^2 < \rho\} \leq \frac{1}{n \log n}.$$

Next, we bound the probabilities of events defined in Lemma S.1.

$$\begin{aligned} \Pr\{\mathcal{E}_n(h, \rho)\} &= 1 - \Pr\{[\mathcal{A}_n(h, \rho)]^c \cup [\mathcal{B}_n(h, \rho)]^c\} \\ &\geq 1 - \Pr\{[\mathcal{A}_n(h, \rho)]^c\} - \Pr\{[\mathcal{B}_n(h, \rho)]^c\}. \end{aligned} \quad (\text{S.1})$$

Now, note that

$$\begin{aligned} \Pr\{[\mathcal{A}_n(h, \rho)]^c\} &= \Pr\{\exists x \in \mathcal{F} : \|G(x, h)\|_2^2 > \rho\} \leq \sum_{x \in \mathcal{F}} \Pr\{\|G(x, h)\|_2^2 > \rho\} \\ &\leq \sum_{x \in \mathcal{F}} \frac{1}{n \log n} \leq n \left(\frac{1}{n \log n} \right) = \frac{1}{\log n}. \end{aligned} \quad (\text{S.2})$$

Similarly,

$$\begin{aligned} \Pr\{[\mathcal{B}_n(h, \rho)]^c\} &= \Pr\{\exists \tau \in \mathcal{J} : \|G(\tau, h)\|_2^2 < \rho\} \leq \sum_{\tau \in \mathcal{J}} \Pr\{\|G(\tau, h)\|_2^2 < \rho\} \\ &\leq \sum_{\tau \in \mathcal{J}} \frac{1}{n \log n} \leq \frac{n}{n \log n} = \frac{1}{\log n}. \end{aligned} \quad (\text{S.3})$$

Combining (S.1), (S.2) and (S.3), we conclude that

$$\Pr\{\mathcal{E}_n(h, \rho)\} \geq 1 - \frac{2}{\log n} \rightarrow 1. \quad (\text{S.4})$$

Finally, the theorem follows from Lemma S.1. \square